Experimental observations of enhanced radial transport of energetic particles with Alfvén eigenmode on the LHD

To cite this article: M. Osakabe *et al* 2006 *Nucl. Fusion* **46** S911

Nucl. Fusion 46 (2006) S911–S917 doi:10.1088/0029-5515/46/10/S07

Experimental observations of enhanced radial transport of energetic particles with Alfvén eigenmode on the LHD

M. Osakabe[1], S. Yamamoto[2], K. Toi[1], Y. Takeiri[1], S. Sakakibara[1], K. Nagaoka[1], K. Tanaka[1], K. Narihara[1] and the LHD Experimental Group

[1] National Institute for Fusion Science, Toki 509-5292, Japan
[2] Graduate School of Enginnering, Osaka University, 2-1 Yamadaoka Suita, Japan

Received 20 February 2006, accepted for publication 24 July 2006
Published 22 September 2006
Online at stacks.iop.org/NF/46/S911

Abstract
Clump and hole creations are observed with TAE bursts in energetic neutral spectra at low-magnetic field configurations of the LHD. Energy slowing down of the clump and the hole are also observed, experimentally. From the slowing down time analysis of the clump and/or hole, the location of each orbit is identified. The drift surface of each orbit has its maximum or second maximum close to the gap location of the TAE burst. The simultaneous observations of clump and hole creations in the energetic spectra reveal the enhanced radial transport of energetic particles by TAE bursts on the LHD.

PACS numbers: 52.55.Pi

1. Introduction

The interactions of Alfvén eigenmodes (AE) on the transport of energetic particles are one of the most important issues in fusion reactor research since their interactions on fusion produced alphas might cause serious problems for the performance of a fusion reactor. The excitations of AE and their interactions with energetic particles are observed in various magnetically confined fusion devices, such as TFTR, JET, DIII-D, W7-AS and so on [1–6].

On the LHD, energetic hydrogen neutral beams, up to 180 keV, are tangentially injected into plasmas. The operational magnetic fields of the LHD range from 0.4 to 3.0 T. These conditions enable us to study the interaction of AE with energetic particles on the LHD [7–11]. During the high-beta experiments of the LHD, the fast change of energetic neutral fluxes with AE bursts were observed on a tangential neutral particle analyser (NPA). The observed changes in energetic neutral spectra indicate the formation of clump–hole pairs in the energetic particle spectra with AE bursts in real space.

Spontaneous creation of clump–hole pairs in energetic particle spectra by AE was shown theoretically by Berk *et al* [12, 13], who pointed out that the pairs are created in the phase space of the spectra and that the down-shift of a clump in its energy and up-shift of a hole correspond to the chirp-down and -up of the mode frequencies, respectively. Within the limits of their theoretical model, Berk *et al* do not make any mention about pair creation in real space.

In this paper, we show experimental observations of the AE interactions on energetic particles on the LHD. The experimental apparatus is shown in section 2. The clump formation in energetic neutral spectra with AE are shown in section 3 and the hole formation is shown in section 4. Section 5 presents the conclusion.

2. Experimetal set-up

Figure 1 shows the schematic drawing of the LHD. On the LHD, NBs are tangentially injected with three NB injectors which are based on the negative-ion sources [14]. Each of the injectors has two ion sources and the tangency radii of these ion-sources are 3.63 m and 3.77 m, respectively. The beams are injected, one for co-direction and the other two for counter-direction at standard LHD magnetic field directions.

To investigate the confinement property of passing energetic particles, an $E//B$-type charge exchange NPA [15] is installed on a tangential port, which is located at 10 cm below the mid-plane. It is placed to measure the counter NB particles for the LHD standard magnetic field direction. The NPA is horizontally movable and its scanning angle ranges from 0° to 9°, where these angles are defined by the angle between the normal of the port and the NPA line-of-sight. In figure 2, the distributions of pitch angles along several NPA

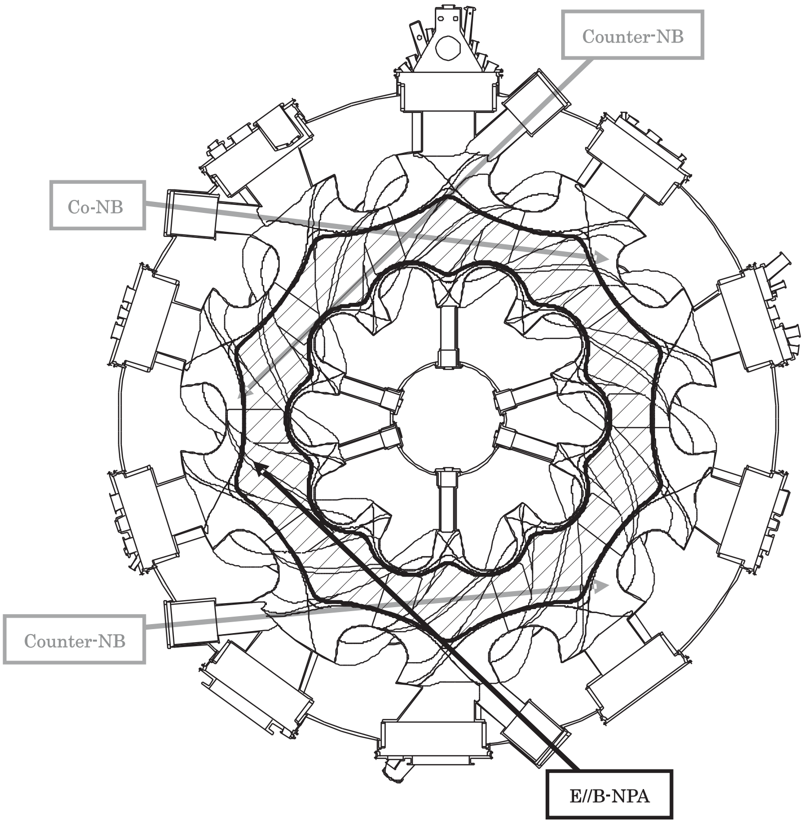

Figure 1. Schematic drawing of LHD configurations.

sight lines are shown as a function of normalized minor radii. The energy range of the NPA is from 0.5 to 200 keV amu^{-1}. The typical time resolution of the measurement is 0.5 ms, which is determined by the typical pulse duration of a plasma discharge at the LHD and the memory size of scaler modules of the NPA.

3. Increase in energetic neutral flux with the TAE burst

In figure 3, typical waveforms of a discharge with MHD bursts are shown together with the change of tangential energetic neutral spectra. The magnetic field strength of the discharge is −0.5 T and the location of the magnetic axis position in the vacuum field is 3.6 m. The negative sign of the magnetic field strength means that the field direction is opposite to the LHD standard configurations; thus the NPA monitors co-passing particles in this discharge. The viewing angle of the NPA is set to 0° in this discharge and sampling rate of the NPA is 2 ms. As shown in figure 3(*e*), the neutrals of high energy components (of around 135 keV) simultaneously increase with the MHD burst signals, which are observed by Mirnov coils. From an analysis of Mirnov coils, the bursts are identified as $n = 2$ TAE. Since the energetic neutral measurements are results of the products of energetic ions in plasmas and the low energy neutrals from plasma peripherals, we must be careful for the behaviour of peripheral neutrals in the evaluation of neutral particle measurement data. If TAE bursts have influences on the peripheral neutral density, the effect should also appear on the H_α signals and the influences on energetic neutral signals

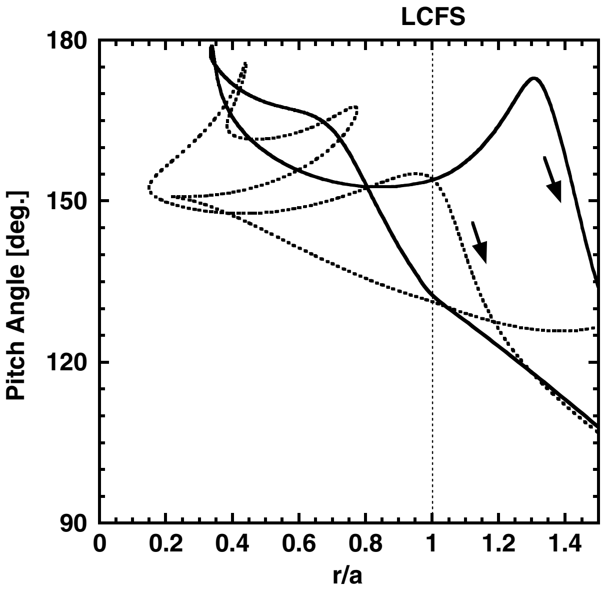

Figure 2. The pitch angle and normalized minor radii (r/a) distributions along the line-of-sight of E//B-NPA for the LHD standard magnetic field configuration ($R_{\rm ax} = 3.6$ m). The solid lines correspond to the 0° NPA line-of-sight, while the dashed lines to the 4° line-of-sight. The viewing angle of the NPA is defined using the angle between the NPA centre line and the normal of the NPA-port flange.

should not have time delays which depend on their energies. As shown in figure 3(*b*), there are no significant influences of TAE bursts on H_α signals. Moreover, the increases in lower energy neutrals (40–100 keV) have certain delay times from

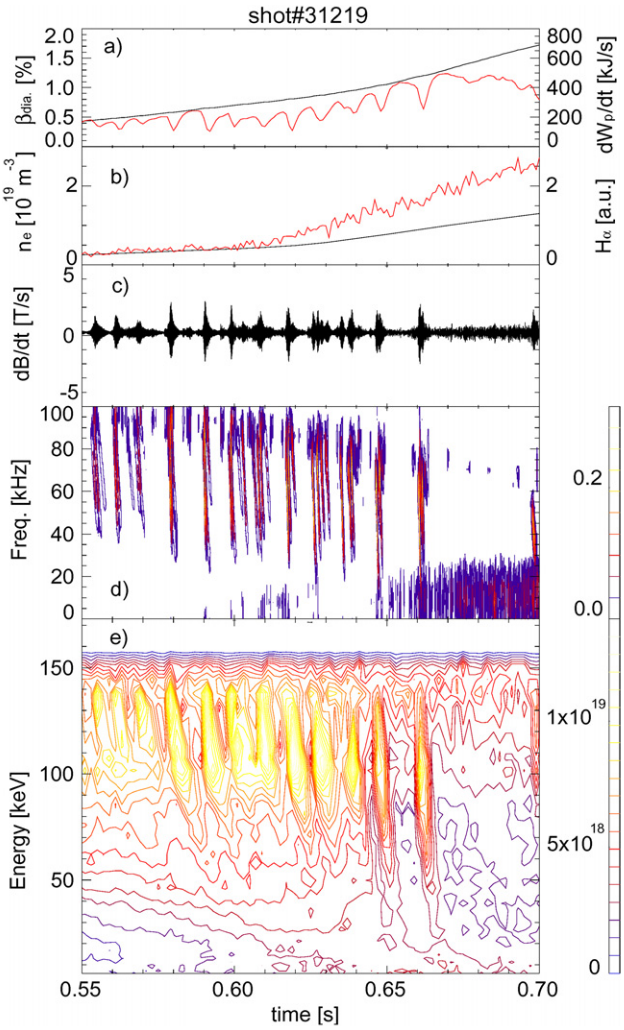

Figure 3. Typical waveforms of a discharge when the change of energetic neutrals are observed with TAE burst signals. (*a*) Diamagnetic beta values (black lines) and time derivative of plasma stored energy (red lines), (*b*) line averaged electron densities (black lines) and H_α-signals (red lines) are shown. (*c*) The signals of mirnov coils are shown. (*d*) Its frequency spectra are shown using contour lines. (*e*) The behaviour of tangential energetic neutral spectra are also shown by contour lines. The NPA viewing angle is set to 0° in this discharge.

the bursts. Therefore, the flux increase in these energetic neutrals is considered to be a result of the change in energetic ion population on the NPA line-of-sight.

Since the increase in energetic neutrals in the low energy range (40–100 keV) does not change simultaneously with the TAE burst and the delay times become longer as the energies become lower, it is considered that the flux increase in this energy range is not directly connected to the burst and is simply a result of classical slowing down of a clump of energetic particles which is formed by the burst. In figure 4, the characteristic times of the delay are compared with the line averaged electron densities ($\bar{n}_e$) at the burst timing. The characteristic times of the delay are evaluated from an exponential fitting of peak-locations at each of the energy channels of the NPA. These characteristic times are scaled as $\bar{n}_e^{-1.3}$, which is close to the inverse of $\bar{n}_e$. This indicates

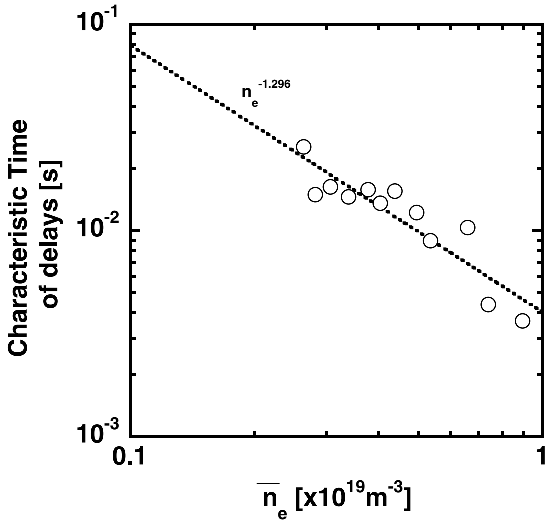

Figure 4. Charateristics times of the delay are plotted by open circles against the line averaged electron densities at the burst timing. The dashed line shows the fitting result of them to the power of $\bar{n}_e$, and is scaled as $\bar{n}_e^{-1.296}$.

that the characteristic time is related to the energy slowing down process. In figure 5(*a*), the characteristic times are compared with the energy slowing down times of hydrogen ions, which circulate on the orbits tangent to the NPA line-of-sight. The slowing down times are averaged over the orbits of these ions. The characteristic times of the delay have good correlations with the slowing down time of particles on the orbit of $\langle r/a\rangle_{\mathrm{orbit}} = 0.55$, where the symbol '$\langle\rangle_{\mathrm{orbit}}$' indicates the average over the orbit. This fact confirms that the delay times in the flux increase at lower energies are due to the result of the slowing down process of energetic ions. Using these energy slowing down time distributions, the location of orbits, where the particles circulate after the influence of TAE bursts, can be identified and are shown in figure 5(*b*). As is expected from figure 5(*a*), the locations are well localized at a certain region in minor radii. This means the clump of energetic particles are formed by the interaction with a particular TAE.

The particle location being identified by the delay time is compared with shear Alfvén spectra in figure 6. At $t = 0.94$ s in this discharge, clump formations in the energetic neutral spectra are observed with the burst of magnetic fluctuations. The frequency of the burst is 50 kHz and the dominant mode is $n = 1$(toroidal)/$m = 1$(poloidal) in this case. The peak position at each energy channel of the NPA is shown in figure 6(*b*). The slowing down time of the clump is estimated to be 3.1 ms by an exponential fitting of these peaks. The slowing down time distribution along the NPA line-of-sight is shown in figure 6(*c*), where the energy slowing down of a proton from 86 to 54 keV is calculated and averaged over its orbit. The slowing down time of the clump becomes 1.3 ms in this figure, which corresponds to the exponential energy decay time of 3.1 ms. Thus, the location of the clump formation is evaluated to be around $\langle r/a\rangle_{\mathrm{avg.}} = 0.65$. Since the magnetic field strength ($B_{\mathrm{ax}} = 0.5$ T) was very low in this discharge compared with the LHD standard magnetic field strength ($B_{\mathrm{ax}} = {\sim}3$ T), drift surfaces of the proton's orbits being measured by the

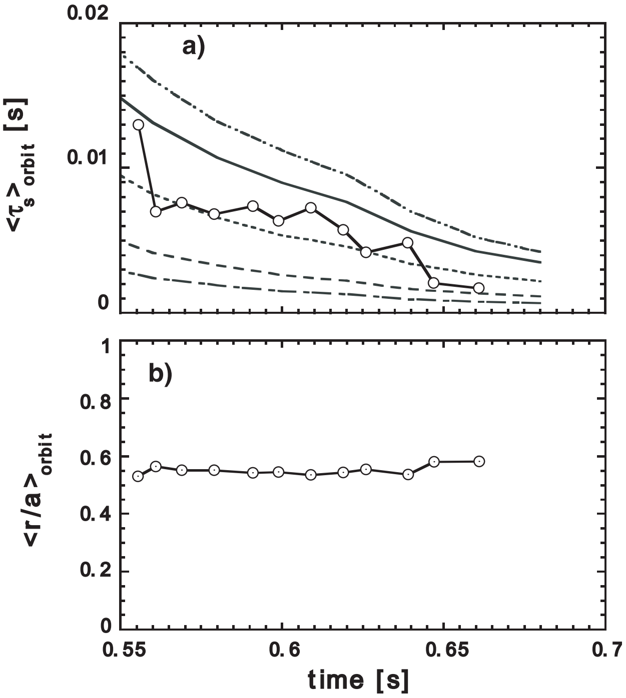

Figure 5. (*a*) Two dotted lines, solid lines, short-dashed lines, long dashed lines, centre dashed lines, show the energy slowing down time of energetic hydrogen ions circulating on the orbit of $\langle r/a\rangle_{\rm avg.} = 0.51, 0.53, 0.55, 0.59$ and 0.64, respectively. The characteristic times of the delay are plotted by lines with open circles. (*b*) The location of the particles which is influenced by the TAE-burst. These locations are evaluated by comparing the characteristic times of the delay to the calculated energy slowing down times.

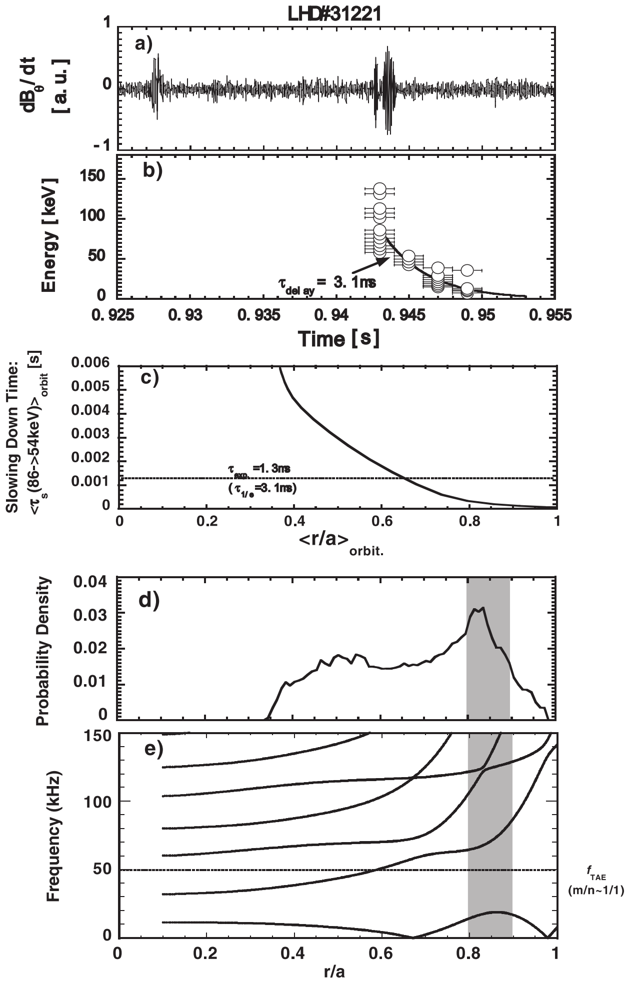

Figure 6. (*a*) The signals of mirnov-coils, (*b*) the peak position of increased flux at each energy channel of the NPA. Dashed lines show the fitted curves of these positions to an exponential function. (*c*) A slowing down time distribution of particles circulating on the NPA line-of-sight. Slowing down times of protons from 86 to 54 keV are calculated and averaged over their orbit, which are tangent to a NPA line-of-sight. The dashed line indicates the slowing down time which corresponds to $\tau_{\rm delay} = 3.08$ ms. (*d*) Probability distribution of a proton staying at certain locations in normalized minor radii. The proton is assumed to circulate on the orbit of $\langle r/a\rangle_{\rm avg.} = 0.65$, which is evaluated from the slowing down time distribution on the NPA line-of-sight. The dashed lines in the figure show the normalized minor radius where the orbit intersects with the NPA line-of-sight. (*e*) Shear Alfvén spectra for $n = 2$ modes. The dashed lines in the figure denote the frequency of the burst at $t = 0.943$ s. The gray areas in these figures express the TAE-gap location for $n = 2/m = 2$ and 3 mode.

NPA deviate significantly from the magnetic flux surfaces. Figure 6(*d*) shows the distribution of the drift surface for the orbit of $\langle r/a\rangle_{\rm avg.} = 0.65$ in normalized minor radius. In the orbit calculation, the energy of the proton is assumed to be 75 keV. The distribution was obtained by calculating the length of time when a proton stays at a certain location in normalized minor radius along its orbit and by normalizing the time with the entire orbit following time. The shear Alfvén spectra for the $n = 1$ mode are also shown in figure 6(*e*). The TAE gap for the $n = 1/m = 1, 2$ mode was located at around $r/a = 0.85$. The frequency of the gap is around 50 kHz, which agrees well with the experimental observation. One of the peaks of the drift surface distribution for $\langle r/a\rangle_{\rm orbit} = 0.65$ is also located around $r/a = 0.85$. It is considered that the clump was formed with the transport of energetic protons in real space by the influence of the TAE. These protons are transported to the orbit of $\langle r/a\rangle_{\rm orbit} = 0.65$ on the NPA line-of-sight from somewhere in the plasma.

4. The observation of a hole formation in the energetic particle spectrum with the TAE burst

The formation of a hole in the NPA spectra is also observed on the LHD. Figure 7 shows typical waveforms of the discharge when a hole formation was observed in energetic particle spectra. The magnetic field strength and the magnetic axis were –0.5 T and 3.6 m, respectively. The NPA viewing angle was 4° in this case. As shown in figure 7, the decrease in energetic neutral flux intensity was observed at around 160 keV right after a burst of Mirnov coil signals. The frequency of the burst was 60 kHz and the toroidal mode number was $n = 1$. Three of the NBs were continuously injected during this time interval. Similar to the case of clump formation, the decreases in energetic neutrals were also observed in the lower energy region with certain delay times. Since there were no significant changes in H_α and electron density waveforms and the decreases had dependence on the energy of neutrals, the decrease in the flux intensity was considered a loss of energetic particles from the NPA line-of-sight. The delay

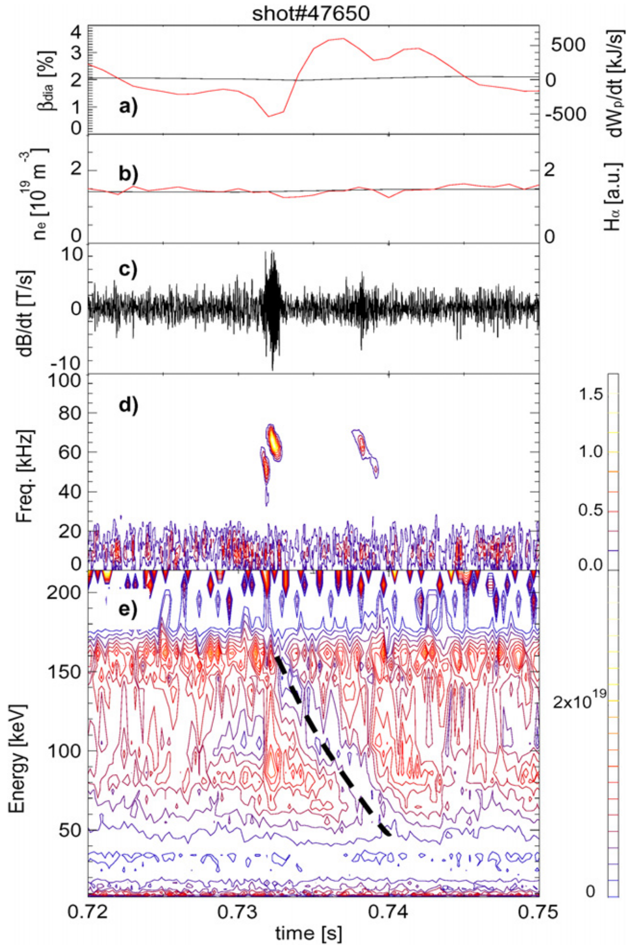

Figure 7. Typical waveforms of a discharge when a hole formation is observed with TAE burst signals in the energetic neutral spectra. (*a*) Diamagnetic beta values (black lines) and time derivative of plasma stored energy (red lines). (*b*) Line averaged electron densities (black lines) and H_α-signals (red lines) are shown. (*c*) The signals of mirnov coils are shown. (*d*) Its frequency spectra are shown using contour lines. (*e*) The behaviour of tangential energetic neutral spectra are also shown by contour lines. The NPA viewing angle is set to 4° in this discharge. The temporal behaviour of the hole in the energetic particle spectra is indicated by dashed lines in (*e*).

times were also considered as a result of the slowing down of the energetic particles which were influenced by the burst and changed their orbit from their original location. Therefore, the original location of the influenced particles could be identified from the energy slowing down time of the hole, which was evaluated to be 7.3 ms from the exponential fitting of the hole locations. In figure 8, the slowing down time distribution is shown for energetic protons on the NPA line-of-sight. The location of the hole is identified to be $\langle r/a\rangle_{\rm avg.} = 0.75$ from this figure. In figure 7, the increase in neutral flux is also observed, but this increased flux is only observed during the burst duration, which means the clump is transported to the prompt loss region of the plasma as shown in the hatched area in figure 8.

The formation of both clump and hole with a burst is simultaneously observed and is shown in figure 9. In the figure, both the clump and hole were formed at $t = 0.577$ s with energy of around 160 keV. The energy slowing down of the

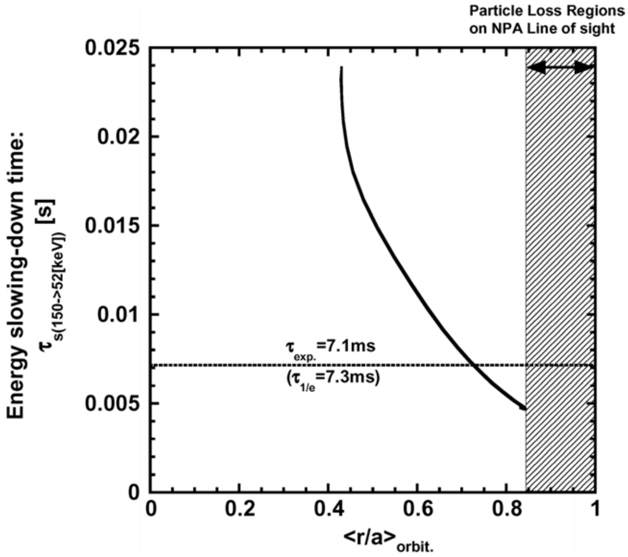

Figure 8. The energy slowing down time distribution along the NPA line-of-sight at $t = 0.73$ s of the discharge shown in figure 7. The energy slowing down time of hydrogen ions from 150 to 52 keV are calculated and averaged over their orbit. The hatched region shows the prompt loss regions on the NPA sight line. The dashed lines in the figure indicate the slowing down time of 7.1 ms, which corresponds to the slowing down time of the hole shown in figure 7(*e*).

clump and hole are indicated by the dotted and dashed lines, respectively, in figure 9(*e*). The $1/e$-holding slowing down time for the clump is 5.2 ms, while that for the hole is 7.6 ms. Using the slowing down time distribution along the NPA sight line, which is shown in figure 10(*a*), the location of the hole and the clump are identified to $\langle r/a\rangle_{\rm orbit} = 0.79$ and 0.91, respectively. The drift surface distributions in the minor radii of each orbit are shown in figure 10(*b*).

In the burst, which is shown in figure 9(*c*), there are two frequency components. One starts from around 60 kHz and chirps down to 50 kHz, quickly. Its mode number is $n = 1/m = \sim 2$. The other starts from around 70 kHz and slowly chirps down to 65 kHz. Its mode number is $n = 1/m = 1$. The mode of $m = 2$ precedes with the mode of $m = 1$. The amplitude of $m = 1$ mode is larger than that of $m = 2$. In figure 10(*c*), the shear Alfvén spectra for the $n = 1$ mode family are shown. The TAE gap for $n = 1/m = 1, 2$ is located at $r/a = \sim 0.7$ and all the burst frequencies are observed within this gap. As is shown in figure 10(*b*), one of the twin lobed peaks of drift surface distribution for the hole orbit is located at the left-hand side of the gap, while that for the clump orbit is at the right-hand side of the gap. This clearly shows the enhanced radial transport of energetic particles by the TAE of $n = 1/m = 1, 2$. Similar to the case of figure 6(*d*), the orbit of influenced particles are chosen so that it has a maximum or second maximum probability of staying near the gap location. In the case of figure 6(*d*), the clump was observed on the orbit which has its outer side peak close to the gap location. On the other hand, in figure 10(*b*), the clump was observed on the orbit whose inner peak is close to the gap location. This difference comes from the fact that our energetic neutral diagnostics is based on passive measurement and from the differences in the orbit topologies of the particles which circulate around the

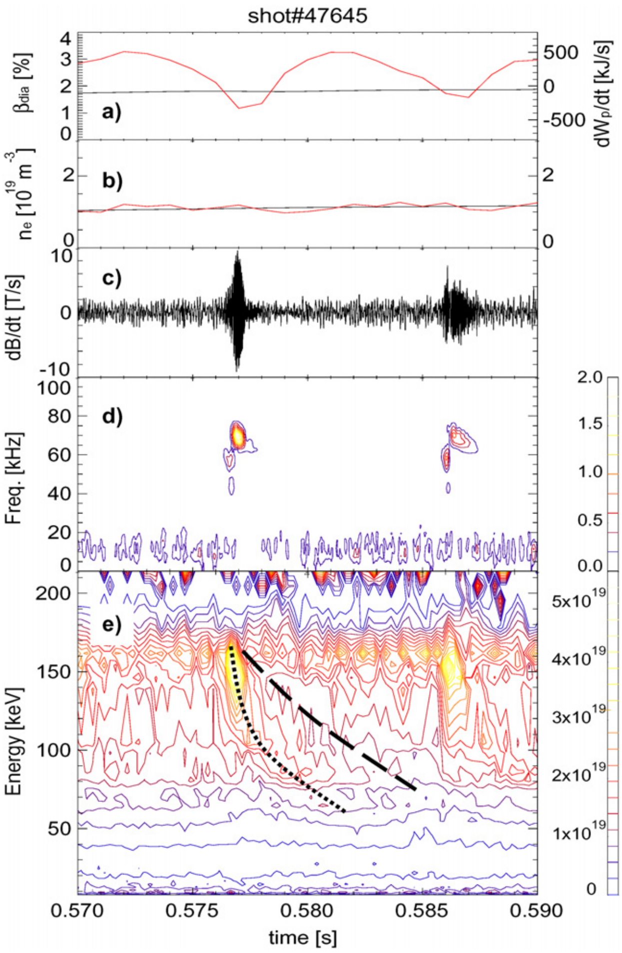

Figure 9. Typical waveforms of a discharge when a hole formation is observed with TAE burst signals in the energetic neutral spectra. (*a*) Diamagnetic beta valuses (black lines) and time derivative of plasma stored energy (red lines). (*b*) Line averaged electron densities (black lines) and H_α-signals (red lines) are shown. (*c*) The signals of mirnov coils are shown. (*d*) Its frequency spectra are shown using contour lines. (*e*) The behaviour of tangential energetic neutral spectra are also shown by contour lines. The NPA viewing angle is set to 1° in this discharge. The temporal behaviour of a clump and a hole in the energetic particle spectra are indicated by dotted lines and dashed lines, respectively.

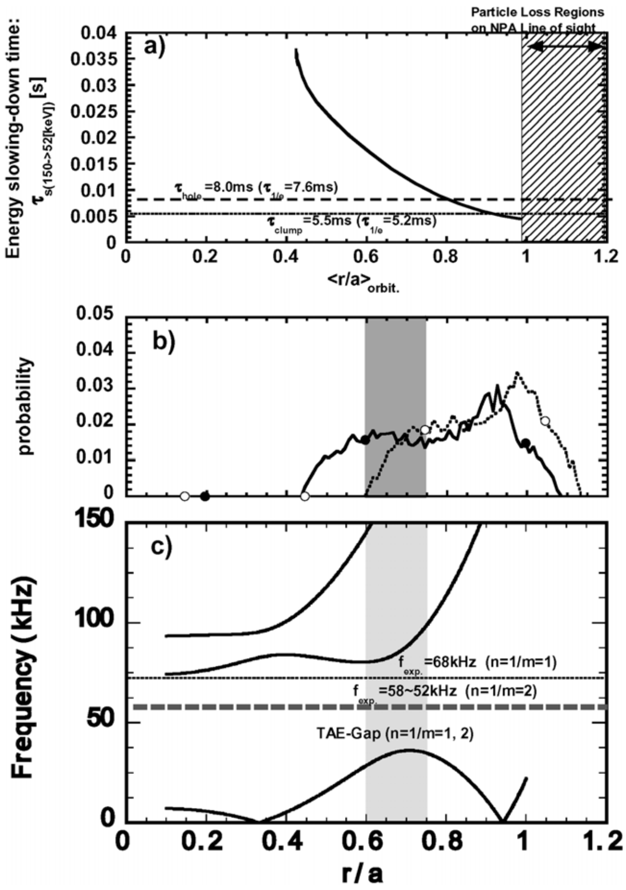

Figure 10. (*a*) The energy slowing down time distribution along the NPA line-of-sight at $t = 0.575$ s of the discharge shown in figure 9. The energy slowing down time of hydrogen ions from 150 to 52 keV are calculated and averaged over their orbit. The hatched region shows the prompt loss regions on the NPA sight line. The dashed lines and centre dashed lines in the figure indicate the slowing down time of the hole (8.0 ms) and the clump (5.3 ms), respectively. (*b*) The drift surface distribution of the orbits for the clump and the hole in the normalized minor radius. (*c*) Shear Alfvén spectra for $n = 1$ modes. The short dashed lines in the figure show the frequency for $n = 1/m = 1$ mode which is identified by the Mirnov signals, while the long dashed lines show that for $n = 1/m = 2$ mode. The gray areas in these figures express the TAE gap location for $n = 1/m = 1$ and 2 modes.

gap locations in each case. In our measurement, energetic neutrals are produced by charge exchange processes between energetic ions in plasmas and low energy neutrals from the plasma peripheral. Since the densities of low energy neutrals are higher at the peripheral than in the centre, it is easier to measure the energetic particles circulating at the outer regions of the plasmas than to measure those at the inner regions, i.e. the clump orbit whose inner peak of the drift surface distribution is located close to the gap is measured more easily than the orbit whose outer peak is close to the gap, as is the case in figure 10(*b*). But, in the case of figure 6(*d*), the gap location is so close to the edge that the clump orbit whose inner peak is close to the gap becomes the prompt loss orbit. Therefore, only the orbit whose outer peak is close to the gap was observed.

Unlike the theoretical prediction of clump–hole pair creation by Berk *et al* [12, 13], the pair creation observed here is in real-space and not in phase-space. We must be careful to determine whether our experimental observations are related to their theory since the simple-radial excursions of particles in a particular energy range could form clump–hole pairs in real space. A better time-resolved measurement of energetic particle spectra during the duration of a TAE burst is necessary to observe the energy shift of a clump and a hole during a frequency chirping process of the mode, which will clarify the relations of our observations to their theory.

5. Conclusion

Changes in energetic neutrals are observed with TAE bursts at low-magnetic field configurations of the LHD. It is found that these phenomena are due to the clump–hole pair creation in the energetic particle spectra by the TAE bursts. The energy slowing down processes of the clumps and the holes are also observed in the energetic neutral spectra. From the slowing down time analysis of the clump or the hole, the location of each orbit is identified. The drift surface distribution of each orbit has twin-lobed peaks, and one of the peaks is close to the TAE gap location of the burst. Simultaneous observation of a clump and a hole formation reveals the enhanced radial transport of energetic particles in plasmas by a TAE burst.

Acknowledgments

The authors wish to thank the Director General of NIFS, Professor Motojima for his continuous encouragement. This work was supported by NIFS2005/ULBB05, and partly supported by the Grant-in-Aid for Young Scientists (A), No 15684012, and for Scientific Research on Priority Areas from MEXT No 16082209.

References

[1] Wong K.L. *et al* 1991 *Phys. Rev. Lett.* **66** 1874
[2] Sharapov S.E. *et al* 1999 *Nucl. Fusion* **39** 373
[3] Heidbrink W.W. *et al* 1991 *Nucl. Fusion* **31** 1635
[4] Duong H.H. *et al* 1993 *Nucl. Fusion* **33** 749
[5] Kusama Y. *et al* 1999 *Nucl. Fusion* **39** 1837
[6] Shinohara K. *et al* 2002 *Nucl. Fusion* **42** 942
[7] Toi K. *et al* 2000 *Nucl. Fusion* **40** 1349
[8] Yamamoto S. *et al* 2003 *Phys. Rev. Lett.* **91** 245001
[9] Toi K. *et al* 2004 *Nucl. Fusion* **44** 217
[10] Yamamoto S. *et al* 2005 *Nucl. Fusion* **45** 326
[11] Toi K. *et al* 2004 *Plasma Phys. Control. Fusion* **46** S1
[12] Berk H.L. *et al* 1997 *Phys. Lett.* A **234** 213
[13] Berk H.L. *et al* 1999 *Phys. Plasmas* **6** 3102
[14] Kaneko O. *et al* 2003 *Nucl.Fusion* **43** 692
[15] Medley S.S. and Roquemore A.L. 1998 *Rev. Sci. Instrum.* **69** 2651